

A Gate-All-Around Single-Channel In₂O₃ Nanoribbon FET with Near 20 mA/μm Drain Current

Zhuocheng Zhang^{1,+}, Zehao Lin^{1,+}, Pai-Ying Liao¹, Vahid Askarpour³, Hongyi Dou², Zhongxia Shang², Adam Chamas¹, Mengwei Si¹, Sami Alajlouni¹, Jinhyun Noh¹, Ali Shakouri¹, Haiyan Wang², Mark Lundstrom¹, Jesse Maassen³, and Peide D. Ye^{1,*}

¹School of Electrical and Computer Engineering, ²School of Materials Science and Engineering, Purdue University, West Lafayette, U.S.A.

³Department of Physics and Atmospheric Science, Dalhousie University, Halifax, NS, Canada

⁺These authors contributed equally to this work *Email: yep@purdue.edu

Abstract

In this work, we demonstrate atomic-layer-deposited (ALD) single-channel indium oxide (In₂O₃) gate-all-around (GAA) nanoribbon FETs in a back-end-of-line (BEOL) compatible process. A maximum on-state current (I_{ON}) of 19.3 mA/μm (near 20 mA/μm) is achieved in an In₂O₃ GAA nanoribbon FET with a channel thickness (T_{IO}) of 3.1 nm, channel length (L_{ch}) of 40 nm, channel width (W_{ch}) of 30 nm and dielectric HfO₂ of 5 nm. The record high drain current obtained from an In₂O₃ FET is about one order of magnitude higher than any conventional single-channel semiconductor FETs. This extraordinary drain current and its related on-state performance demonstrate ALD In₂O₃ is a promising oxide semiconductor channel with great opportunities in BEOL compatible monolithic 3D integration.

Introduction

Amorphous oxide semiconductors are widely investigated and applied as thin-film transistor channels for display applications [1]. Very recently, they are explored for BEOL-compatible transistor channels for monolithic 3D integration [2-5]. Among them, ALD In₂O₃ shows excellent transport properties with mobility beyond 100 cm²/V·s [6] and its FETs exhibit remarkable performance including large on-state current (I_{ON}) over 2-3 mA/μm in both depletion and enhancement-mode operation, on/off ratio up to 10¹⁷, subthreshold swing (SS) as low as 63 mV/dec, and high stability in H₂ environment [6-10]. Meanwhile, the ALD technique offers wafer-scale film synthesis, accurate thickness control, smooth surface, high conformity and uniformity on 3D structures and a low thermal budget process below 300 °C [6-8,11-13].

In this work, for the first time, scaled single-channel In₂O₃ nanoribbon FETs with GAA structure are fabricated under BEOL conditions. I_{ON} is enhanced to 4.3 mA/μm for a channel length (L_{ch}) of 40 nm compared to previous bottom or top-gated ALD In₂O₃ FETs. To resolve the self-heating issue due to the ultrahigh current in the ultrathin channel, the channel width (W_{ch}) is further scaled from 1 μm to 30 nm. The self-heating effect is mitigated significantly after nanoribbon scaling as confirmed by a high-resolution thermo-reflectance (TR) imaging experiment and thermal simulation. A maximum I_{ON} of 19.3 mA/μm is observed in the 30 nm wide nanoribbon FET by pulsed I-V measurements, which further lowers the self-heating effect. This extraordinary drain current density is the highest ever obtained from a single-channel transistor.

Experiments

Fig. 1 shows the device schematic of a single-channel In₂O₃ GAA FET. A fabrication process flow is presented in Fig. 2. The device fabrication started with ALD growth of 10 nm Al₂O₃ at 175 °C to obtain a smooth surface and 40 nm Ni deposition by e-beam evaporation as the bottom gate metal after substrate cleaning. Next, 5 nm HfO₂ bottom dielectric was grown by ALD at 200 °C and 3.1 nm In₂O₃ was grown by ALD at 225 °C with (CH₃)₃In (TMIn) and H₂O as In and O precursors. Channel isolation was done by dry etching (BCl₃: 15 sccm; Ar: 60 sccm; pressure: 0.6 Pa) and Ni was deposited to serve as the source/drain electrodes. A top dielectric of 5 nm HfO₂ was then grown by ALD at 200 °C to wrap the whole In₂O₃ channel followed by 5 min O₂ annealing at 250 °C. Finally, the gate metal was surrounded by e-beam evaporation of 40 nm Ni with dry etching first to connect the top and bottom gates. Fig. 3 shows the EDS cross-section image of an In₂O₃ GAA FET. Single layer In₂O₃ with channel thickness (T_{IO}) of 3.1 nm is surrounded by 5 nm HfO₂ and 40 nm Ni gate stack.

Results and Discussion

Fig. 4 and Fig. 5 present the transfer and output characteristics of a typical In₂O₃ GAA FET with L_{ch} of 1 μm and W_{ch} of 1 μm. Well-behaved switching performance with on/off ratio over 10⁴ and a clear drain current saturation at large V_{DS} are observed. Fig. 6 and Fig. 7 show the transfer and output characteristics of a short channel In₂O₃ GAA FET with L_{ch} of 40 nm and W_{ch} of 1 μm. A maximum I_{ON} of 4.3 mA/μm is achieved at V_{DS} of 1 V. Further increasing V_{DS} results in the device becoming unstable due to ultrahigh current density induced Joule heating in the nanometer-thin In₂O₃ channel. The threshold voltage (V_T)

and transconductance (g_m) scaling metrics of the In₂O₃ FETs are shown in Fig. 8. V_T is near constant and maximum g_m exceeds 10³ μS/μm.

Channel width scaling of the ribbon is also investigated. Fig. 9 illustrates a false-color top-view SEM image of a fabricated GAA In₂O₃ nanoribbon FET with W_{ch} of 50 nm. Electrical measurements are performed and the extracted I_{ON} versus W_{ch} of different devices from 1 μm down to 30 nm is plotted in Fig. 10 with subthreshold swing (SS) of 100-120 mV/dec. It is surprising that I_{ON} is approximately three times larger as the channel narrows. Two factors might account for such current enhancement. First, the electric field induces a higher carrier density at the channel edge due to the GAA geometry and the edge gradually takes a larger portion of the conductance in the channel width scaling. Etched In₂O₃ ribbon edges lead to a charge neutrality level (CNL) located even deeper inside the conduction band, thereby enhancing edge conduction. Second, better heat dissipation is realized in a narrower ribbon. Fig. 11 and Fig. 12 present the transfer and output characteristics of an In₂O₃ FET with L_{ch} of 40 nm and W_{ch} of 30 nm. A maximum I_{ON} of 11.4 mA/μm is achieved at a V_{DS} of 1 V.

A high-resolution TR measurement is conducted to quantitatively investigate the self-heating effect [12]. The device is illuminated by LED pulses with a synchronized charge coupled device camera to capture the surface reflectance, which is then transformed into a temperature scale. Fig. 13 shows the experimental and simulated results of the temperature increase ΔT across the channel of an In₂O₃ GAA FET with L_{ch} of 400 nm, W_{ch} of 1 μm, V_{DS} at 1.4 V and power density of 1.94 kW/mm². Thermal simulation is carried out by the finite-element method using COMSOL. A good agreement is found between experiment and simulation with a maximum ΔT of 23.6 K. To compare with narrow devices, Fig. 14 presents the experimental and simulated results of another In₂O₃ GAA nanoribbon FET with W_{ch} of 200 nm and the same V_{DS} bias. It can be seen that the maximum ΔT reduces to 5.1 K due to better heat dissipation in the smaller nanoribbon. Fig. 15 shows the simulated 2D ΔT results of the smallest In₂O₃ GAA nanoribbon FET, with L_{ch} of 40 nm and W_{ch} of 30 nm, in which a negligible ΔT of 1.1 K is achieved. The excellent transport properties of In₂O₃ remain unchanged in scaled nanoribbon devices.

To further probe the potential of the device performance, a pulsed I-V measurement is implemented. A data averaging time of 500 ns, V_{GS} and V_{DS} pulse width of 1 μs and pulse period of 100 ms are set to minimize the self-heating effect and improve device reliability. Fig. 16 and Fig. 17 present the pulsed transfer and output characteristics of an In₂O₃ GAA nanoribbon FET with L_{ch} of 40 nm and W_{ch} of 30 nm. A record high I_{ON} of 19.3 mA/μm is achieved at V_{DS} of 1.7 V, demonstrating the remarkable current carrying capacity of ALD In₂O₃. The off-state current in the transfer curve is limited by the resolution of the pulsed I-V method while a real on/off ratio over 10⁶ is shown in Fig. 11. DFT simulations [13] of a 3.0 nm thick slab of In₂O₃ were performed to study its electronic properties. Fig. 18 shows the band structure of the conduction states. Fig. 19 presents the ballistic current density and average electronic velocity versus carrier concentration, indicating that an I_{ON} of 20 mA/μm with high velocity >3×10⁷ cm/s can be achieved with an electron density of 4×10¹³ cm⁻² [14].

Conclusion

In summary, single-channel In₂O₃ GAA nanoribbon FETs are demonstrated in a BEOL compatible process. A record high I_{ON} of 19.3 mA/μm is achieved through channel width scaling and improved heat dissipation in small devices. This work demonstrates the great potential of ALD In₂O₃ as a novel channel material in monolithic 3D integration.

The work is supported by SRC nCore IMPACT, DARPA/SRC JUMP ASCENT, AFOSR, NSERC and Compute Canada.

Reference: [1] K. Nomura et al., *Nature*, p. 488, 2004. [2] S. Li et al., *Nat. Mater.*, p. 1091, 2019. [3] M. Si et al., *ACS Nano*, p. 11542, 2020. [4] S. Samanta et al., *VLSI*, p. TH2.3, 2020. [5] W. Chakraborty et al., *VLSI*, p. TH2.1, 2020. [6] M. Si et al., *VLSI*, p. TF2.4, 2021. [7] M. Si et al., *IEEE TED*, p. 1075, 2021. [8] M. Si et al., *IEEE EDL*, p. 184, 2021. [9] P.-Y. Liao et al., *IEEE TED*, p. 147, 2022. [10] A. Chamas et al., *Appl. Phys. Lett.*, p. 263503, 2021. [11] M. Si et al., *Nat. Electron.*, 2022. [12] P.-Y. Liao et al., *VLSI*, 2022. [13] P. Giannozzi et al., *J. Phys.: Cond. Mat.*, vol. 21, p. 395502, 2009. [14] Z. Lin et al., to be submitted.

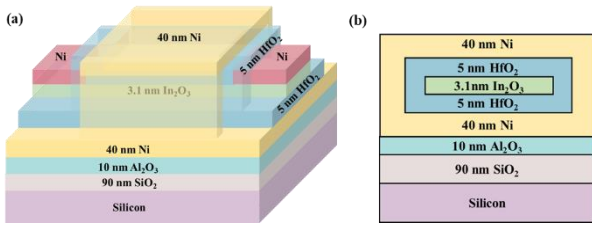


Fig. 1. Device schematic of an In_2O_3 GAA nanoribbon FET with T_{IO} of 3.1 nm and dielectric of 5 nm HfO_2 in (a) 3D model (b) cross-section view in S/D direction.

- SiO_2/Si substrate cleaning
- ALD 10 nm Al_2O_3 at 175 °C
- 40 nm Ni deposition
- ALD 5 nm HfO_2 at 200 °C
- ALD In_2O_3 at 225 °C
- Dry etching to define S/D
- Ni deposition as S/D contact
- ALD 5 nm HfO_2 at 200 °C as dielectric
- O_2 annealing at 250 °C for 5 min
- Dry etching for connection of gate metal
- 40 nm Ni deposition as surrounding gate

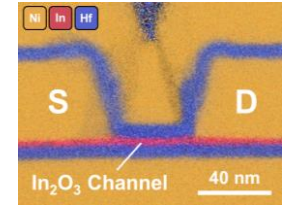


Fig. 2. Fabrication process flow of the In_2O_3 GAA nanoribbon FETs.

Fig. 3. EDS cross-section image of an In_2O_3 GAA FET with L_{ch} of 40 nm.

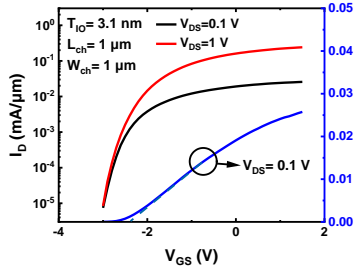


Fig. 4. Transfer characteristics of a typical In_2O_3 GAA nanoribbon FET with L_{ch} of 1 μm and W_{ch} of 1 μm .

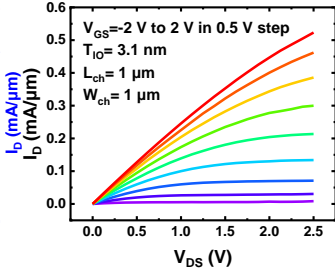


Fig. 5. Output characteristics of a typical In_2O_3 GAA nanoribbon FET with L_{ch} of 1 μm and W_{ch} of 1 μm , showing saturation at large V_{DS} .

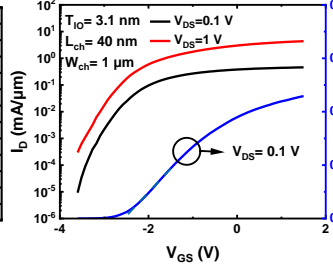


Fig. 6. Transfer characteristics of a typical In_2O_3 GAA FET with L_{ch} of 40 nm and W_{ch} of 1 μm .

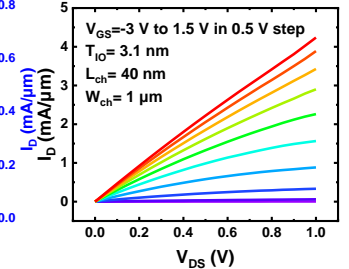


Fig. 7. Output characteristics of a typical In_2O_3 GAA FET with L_{ch} of 40 nm and W_{ch} of 1 μm , showing maximum I_{ON} of 4.3 $\text{mA}/\mu\text{m}$ at $V_{\text{DS}} = 1 \text{ V}$.

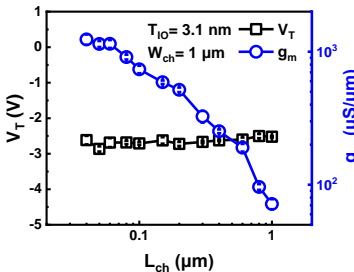


Fig. 8. V_{T} and g_{m} scaling metrics of In_2O_3 GAA FETs with L_{ch} from 40 nm to 1 μm and W_{ch} of 1 μm . g_{m} is extracted at $V_{\text{DS}} = 1 \text{ V}$.

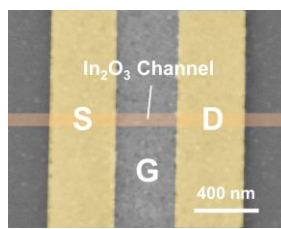


Fig. 9. False-color top-view SEM image of an In_2O_3 GAA nanoribbon FET with W_{ch} of 50 nm.

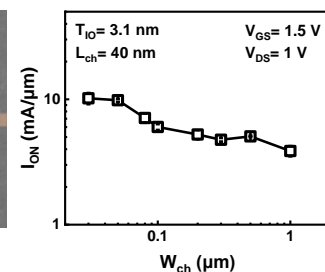


Fig. 10. I_{ON} of the In_2O_3 GAA nanoribbon FETs under channel width scaling from 1 μm down to 30 nm. Each W_{ch} data is from 5-10 devices.

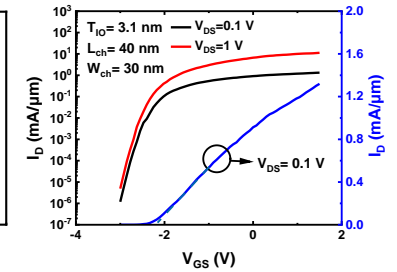


Fig. 11. Transfer characteristics of a typical In_2O_3 GAA nanoribbon FET with L_{ch} of 40 nm and W_{ch} of 30 nm.

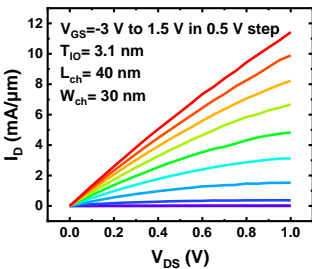


Fig. 12. Output characteristics of an In_2O_3 GAA nanoribbon FET with W_{ch} of 30 nm, showing maximum I_{ON} of 11.4 $\text{mA}/\mu\text{m}$ at $V_{\text{DS}} = 1 \text{ V}$.

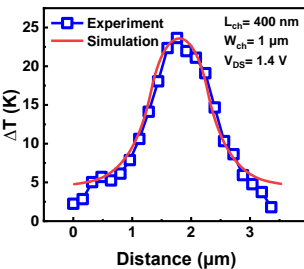


Fig. 13. Cross-sections of the experimental and simulated results of temperature increase ΔT of an In_2O_3 GAA nanoribbon FET with W_{ch} of 1 μm .

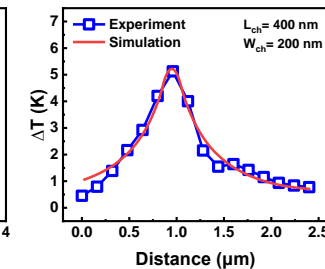


Fig. 14. The same TR measurements and simulations of a device with W_{ch} of 200 nm. Space resolution is limited to hundreds of nm for TR measurement.

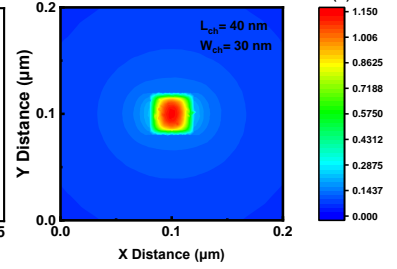


Fig. 15. Simulation result of an In_2O_3 GAA nanoribbon FET with L_{ch} of 40 nm and W_{ch} of 30 nm, showing little temperature increase.

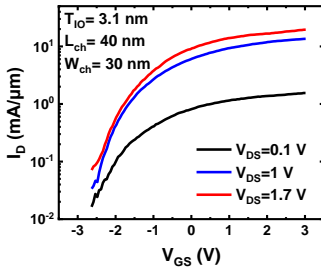


Fig. 16. Pulsed I-V results of transfer characteristics of an In_2O_3 GAA FET with L_{ch} of 40 nm and W_{ch} of 30 nm.

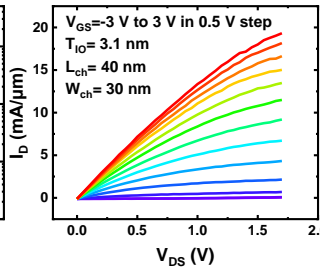


Fig. 17. Pulsed I-V results of output characteristics of an In_2O_3 GAA FET, showing maximum I_{ON} of 19.3 $\text{mA}/\mu\text{m}$.

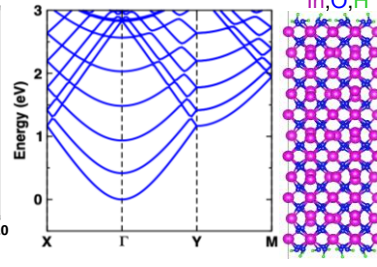


Fig. 18. DFT band structure of 3.0 nm thick In_2O_3 slab, with the lowest conduction band having an effective mass of 0.19 m_0 .

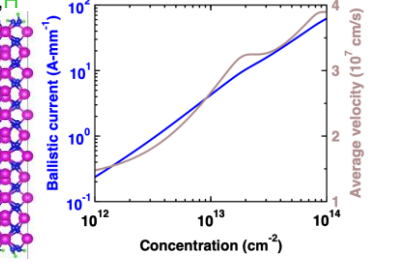


Fig. 19. Ballistic current density and average electron velocity versus carrier density, from DFT simulation of In_2O_3 slab.